Applied Physics Letters ARTICLE pubs.aip.org/aip/apl

Ultrawide bandgap semiconductor heterojunction p–n diodes with distributed polarization-doped p-type AlGaN layers on bulk AlN substrates

Cite as: Appl. Phys. Lett. **124**, 102109 (2024); doi: 10.1063/5.0189419
Submitted: 28 November 2023 · Accepted: 27 February 2024 ·
Published Online: 8 March 2024

Shivali Agrawal,[1,a)] Len van Deurzen,[2] Jimy Encomendero,[3] Joseph E. Dill,[2] Hsin Wei (Sheena) Huang,[3] Vladimir Protasenko,[3] Huili (Grace) Xing,[3,4,5] and Debdeep Jena[2,3,4,5]

AFFILIATIONS

[1]Department of Chemical and Biomolecular Engineering, Cornell University, Ithaca, New York 14853, USA
[2]School of Applied and Engineering Physics, Cornell University, Ithaca, New York 14853, USA
[3]Department of Electrical and Computer Engineering, Cornell University, Ithaca, New York 14853, USA
[4]Department of Materials Science and Engineering, Cornell University, Ithaca, New York 14853, USA
[5]Kavli Institute at Cornell for Nanoscale Science, Cornell University, Ithaca, New York 14853, USA

[a)]**Author to whom correspondence should be addressed:** sa2368@cornell.edu

ABSTRACT

Ultrawide bandgap heterojunction p–n diodes with polarization-induced AlGaN p-type layers are demonstrated using plasma-assisted molecular beam epitaxy on bulk AlN substrates. Current–voltage characteristics show a turn-on voltage of $V_{bi} \approx 5.5$ V, a minimum room temperature ideality factor of $\eta \approx 1.63$, and more than 12 orders of current modulation at room temperature. A stable current operation of the ultrawide bandgap semiconductor diode is measured up to a temperature of 300 °C. The one-sided n^+–p heterojunction diode design enables a direct measurement of the spatial distribution of polarization-induced mobile hole density in the graded AlGaN layer from the capacitance–voltage profile. The measured average mobile hole density is $p \sim 5.7 \times 10^{17}$ cm^{-3}, in close agreement with what is theoretically expected from distributed polarization doping. Light emission peaked at 260 nm (4.78 eV) observed in electroluminescence corresponds to interband radiative recombination in the n^+ AlGaN layer. A much weaker deep-level emission band observed at 3.4 eV is attributed to cation-vacancy and silicon complexes in the heavily Si-doped AlGaN layer. These results demonstrate that distributed polarization doping enables ultrawide bandgap semiconductor heterojunction p–n diodes that have wide applications ranging from power electronics to deep-ultraviolet photonics. These devices can operate at high temperatures and in harsh environments.

Aluminum gallium nitride (AlGaN)-based p–n junction diodes are promising devices for advancing high-power electronics and deep-ultraviolet (UV) photonics. These applications are enabled by the following desirable properties of the AlGaN semiconductor alloy system: a large tunable direct energy bandgap (3.4–6.2 eV), high critical electric field (3–15 MV/cm), and high thermal conductivity (260–340 W/m K), among others. p-type doping is the major bottleneck in realizing a p–n junction using these ultrawide bandgap (UWBG) semiconductors. The acceptor ionization energy of magnesium (Mg) increases with the energy bandgap from GaN [$E_a \sim 200$ meV (Refs. 1 and 2)] to AlN [$E_a \sim 630$ meV (Ref. 3)]. Recent reports on p-type doping of AlN with lower acceptor binding energies and new shallow dopants like Be are under further investigation.[4,5]

Deep acceptors with $E_a \gg k_bT$, where k_b is the Boltzmann constant and T is the temperature, lead to poor ionization, low free carrier concentrations, and increased on-resistance in the diode p-type region. The large disparity between electron and hole carrier concentration and mobility causes an efficiency droop in light-emitting diodes (LEDs).[6] Several allied limitations with using a high concentration of Mg in active regions include surface polarity inversion,[7,8] Mg precipitation,[9] surface segregation,[10] self-compensating defects formation,[11] memory effects,[12] and increased frequency dispersion in diodes,[13] among others. In the design of waveguides for deep-UV laser diodes, Mg-doped cladding layers are undesirable because they cause high Mg-induced optical losses that increase the threshold gain.[14]

One way to overcome these challenges is to leverage the spontaneous and piezoelectric polarization of wurtzite III/V nitride semiconductors. Spatial compositional grading of AlGaN along the polar axis creates a *fixed* bulk three-dimensional (3D) polarization bound charge,

whose electric field enables the formation of *mobile* three-dimensional charges of opposite polarity. The use of such distributed polarization-doped (DPD) layers has played a key role in the demonstration of deep-UV laser diodes,[15–18] LEDs,[19,20] and power diodes.[21–24] In this work, we create a DPD p-type layer by linearly grading down the AlGaN composition along the +c direction of the crystal. The grading creates a three-dimensional hole gas.[25–27] We use a one-sided n^+–p heterojunction to measure the spatial density profile of the 3D hole gas. We also find that the resulting ultrawide bandgap heterojunction diode current–voltage characteristics exhibit close to unity ideality factor, stable high-temperature operation, and electroluminescence.

Space-charge profiling of DPD-based diodes grown on bulk AlN was recently reported in metal organic chemical vapor deposition (MOCVD) grown diodes.[28] There are no reports of such measurements on molecular beam epitaxial (MBE) grown devices. MBE offers some differences from MOCVD, such as lower growth temperature, lower hydrogen incorporation, and the absence of memory effects, enabling precise dopant profiles and sharp heterointerfaces. While MBE grown two-dimensional (2D) hole gases were demonstrated on single-crystal AlN bulk substrates,[29] polarization-induced 3D hole gases on bulk AlN have not been realized yet. In this study, we present an MBE grown quasi-vertical p–n diode that uses an undoped distributed polarization-doped layer for hole injection. We find an average mobile hole concentration of 5.7×10^{17} cm^{-3}, consistent with what is expected from spontaneous and piezoelectric polarization effects. These findings make unintentionally doped (UID) DPD-based diodes an attractive alternative to the conventional impurity-based pn diodes.

The diode heterostructures were grown in a nitrogen plasma-assisted Veeco Gen10 molecular beam epitaxy (MBE) system on +c-plane single-crystal bulk AlN substrates. The substrates were subjected to two essential cleaning steps as described in detail elsewhere:[30,31] (1) an *ex situ* cleaning using solvents and acids and (2) an *in situ* cleaning achieved through repeated cycles of Al adsorption and desorption, referred to as Al-assisted polishing. These steps eliminate the native surface oxides to enable high-quality homoepitaxy.

As shown in Fig. 1(a), a 500 nm thick AlN buffer layer was grown at a high temperature of $T_{sub} \sim 1060$ °C in Al-rich conditions to isolate the device layers from remaining substrate surface impurities. The subsequent AlGaN epilayer was grown under Ga-rich conditions at a lower substrate temperature of 880 °C to enhance Ga incorporation. Excess metal was thermally desorbed at the end of each layer to ensure sharp heterojunctions. From bottom to top along the metal-polar growth direction, the targeted p–n diode heterostructure, as seen in Fig. 1(a), consists of (1) a 500 nm MBE grown AlN buffer layer, (2) a 400 nm $Al_{0.7}Ga_{0.3}N$ layer with Si doping density $N_d \approx 3 \times 10^{19}$ cm^{-3}, which resulted in a free electron density $n \approx 2 \times 10^{19}$ cm^{-3} at room temperature from Hall-effect measurements, (3) an unintentionally doped (UID) DPD layer linearly graded from $Al_{0.95}Ga_{0.05}N$ to $Al_{0.65}Ga_{0.35}N$ over 300 nm, and followed by (4) a 50 nm heavily Mg-doped GaN capping layer to form the metal p-contacts. In the entire device stack, Mg impurity doping is only incorporated in the GaN p-contact layer and not in the Al containing UWBG layers.

Following the epitaxy of the device heterostructures, the layers were fabricated into quasi-vertical diodes as indicated in Fig. 1(a) and shown in Fig. 1(b). First, circular device mesas were formed by chlorine-based inductively coupled plasma reactive ion etching (ICP-RIE) with a total etch depth extending 100 nm into the n-type AlGaN layer. The device mesa diameters range from 20 to 400 μm. Then, n-type metal–semiconductor contacts were formed by electron beam evaporation of a V/Al/V/Au stack with thicknesses of 20/80/40/100 nm, which was subsequently rapid thermal annealed (RTA) at 800 °C for 60 s in an N_2 ambience. Finally, p-type metal–semiconductor Ni/Au contacts with thicknesses of 15/20 nm were deposited by electron beam evaporation and annealed by RTA at 450 °C for 30 s in an O_2 environment. A 20/100 nm Ti/Au metal stack was subsequently deposited by electron beam evaporation for probing. Electrical measurements were performed using a Keithley 4200A semiconductor parameter analyzer. Electroluminescence spectra were collected using a Princeton Instruments spectrometer with 2400 grooves/mm and a blaze wavelength of 240 nm. All measurements were performed on devices with a 104 μm diameter, unless specified otherwise. Figure 1(a) shows a cross-sectional view of the device, and Fig. 1(b) shows a scanning electron microscope (SEM) image of the fabricated device at a 45° tilt. The SEM was taken by a Zeiss ULTRA microscope at a 5 kV beam voltage with an in-lens detector.

Figure 1(c) shows atomic steps on the top p-GaN layer of the as-grown sample with a root mean square roughness of 0.33 nm over 2×2 μm^2 scan area measured by atomic force microscopy (AFM), confirming step flow growth mode throughout the structure. The x-ray diffraction (XRD) scans in Fig. 1(d), performed using a

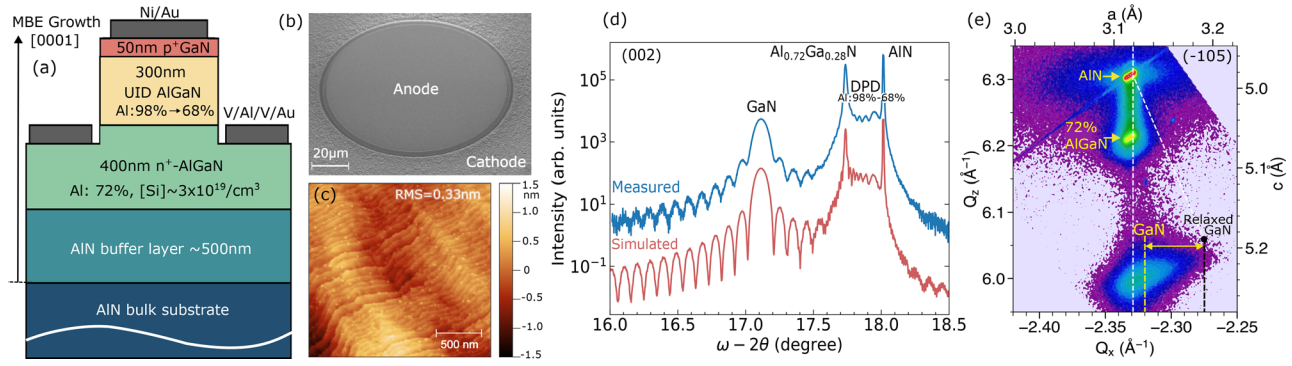

FIG. 1. (a) Cross-sectional view of the fabricated device structure in this study. (b) SEM image of a 104 μm diameter device. (c) 2×2 μm^2 AFM micrographs of the top GaN surface of the as-grown sample indicating the smooth surface and two-dimensional growth mode. (d) Measured and simulated $2\theta - \omega$ XRD scans of the sample across the (002) diffractions. (e) RSMs across the asymmetric ($\bar{1}05$) diffractions.

Panalytical Empyrean system, show good agreement between the measured and simulated $2\theta - \omega$ XRD scans of the sample across the (002) diffractions. The actual Al compositions found from XRD are 2%–3% higher than the targeted structure. The reciprocal space map (RSM) around the asymmetric $(\bar{1}05)$ diffractions in Fig. 1(e) shows that the AlGaN layers are fully strained to the AlN, while the GaN layer is relaxed and has an in-plane lattice strain of approximately 1.9%.

Figure 2(a) shows the room temperature current–voltage characteristics of the diode. The reverse bias leakage current detection is limited by the 100 fA noise floor of the equipment until approximately −8 V, beyond which it increases gradually. In the forward bias, the diode turn-on voltage is approximately 5.5 V, and a specific on-resistance of 0.9 Ω cm^2 at 6 V. The maximum measured forward current density of 1.3 kA/cm^2 at ∼20 V was limited by the current limit of the equipment. The measured 12 orders of current modulation (limited by the measurement noise floor and compliance) illustrate the capability of the AlGaN heterojunction p–n diode without Mg doping in the AlGaN layers.

Figure 2(b) shows the turn-on behavior in linear scale and the corresponding ideality factor. The diode forward current is[32] $J_F \approx J_0 \exp[qV/(\eta k_b T)]$, where J_0 is a voltage-independent and material-dependent coefficient, q is the electron charge, V is the junction voltage, and η is the ideality factor. $\eta = 2$ when non-radiative Shockley–Read–Hall interband recombination current is dominant, and $\eta = 1$ when minority carrier diffusion current dominates. The voltage-dependent ideality factor from the general diode relation,

$$\eta = \frac{q}{k_b T} \times \frac{dV}{d\ln(J/J_0)}, \tag{1}$$

is used to obtain the η shown in Fig. 2(b). η reaches a minimum value of approximately 1.63 in a narrow voltage range around 4 V near turn on, one of the lowest reported to date in ultrawide bandgap pn diodes. The deviation of the experimental ideality factor from the theoretical models ($1 \leq \eta \leq 2$) in AlGaN/GaN p–n junction diodes has been attributed to non-ohmic metal–semiconductor junctions.[21,33] By performing transfer length method (TLM) measurements, we found that both the p and n contacts are not entirely ohmic and exhibit some non-linearity. In this case, the total ideality factor is the sum of individual ideality factors of all the rectifying junctions in the system, as derived by Shah *et al.*[33] The presence of the Schottky-like contact diodes in series with the pn junction diode, therefore, complicates an accurate determination of the true ideality factor of the p–n junction itself.

Figures 2(c) and 2(d) show the temperature dependence of the diode current from 25 to 300 °C. The reverse leakage current in Fig. 2(c) increases with increasing electric field and temperature. This is a signature of trap-assisted tunneling being the dominant leakage mechanisms, such as the Frenkel–Poole (FP) process[34] or variable-range hopping (VRH).[35] A far more dramatic temperature dependence is observed in the forward bias current in Fig. 2(d). For example, at a forward bias of 3.5 V, the current density increases by 5 orders of magnitude when the temperature is increased from 25 to 300 °C. A large exponential increase in current is indeed expected with temperature because the intrinsic interband thermally generated carrier density is $n_i \propto \exp(-E_g/(2k_bT))$, and in the ideal diode theory, $J_0 \propto n_i^2 \propto \exp(-E_g/(k_bT))$ is a strong function of temperature. The minimum ideality factor increased to 2.0 at 300 °C, which could be due to heat or current induced degradation to the device, resulting in an increased recombination current. Stress induced degradation has been shown to result in an increased point defect density in UV LEDs.[36,37]

Figure 3(a) shows the calculated energy band diagram of the pn heterojunction diode at zero bias, highlighting the depletion region. Unlike in non-polar pn diodes, at this polar AlN/AlGaN p–n heterojunction, there is no depletion region in the n-side. Across the heterointerface of n-$Al_{0.72}Ga_{0.28}N$ and AlN, there is a polarization discontinuity and an energy band discontinuity. Since the n-AlGaN is

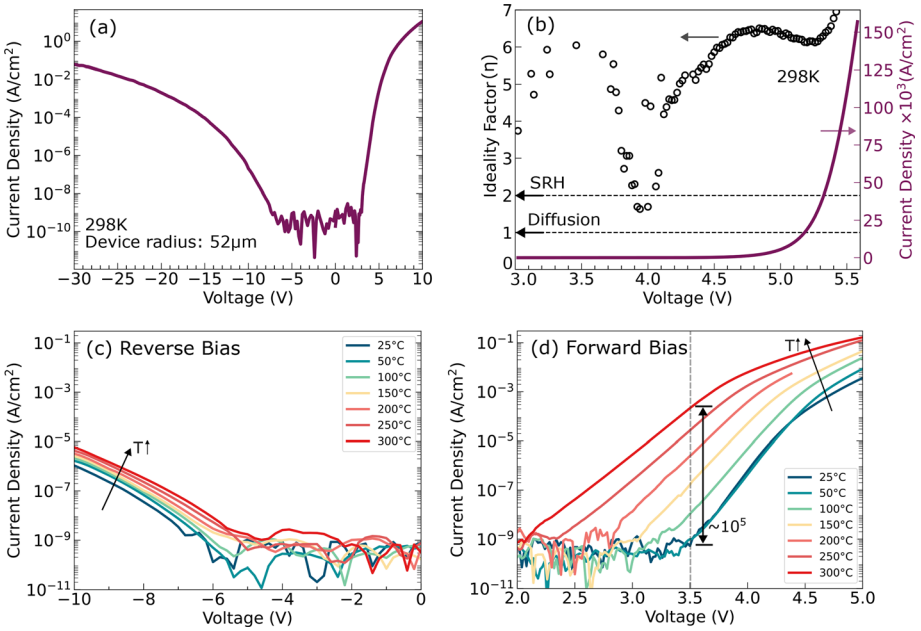

FIG. 2. (a) Room temperature J–V characteristics of the diode. (b) The extracted ideality factor from (a) using Eq. (1). (c) Temperature dependent J–V characteristics in reverse bias. (d) Temperature dependent J–V characteristics in forward bias.

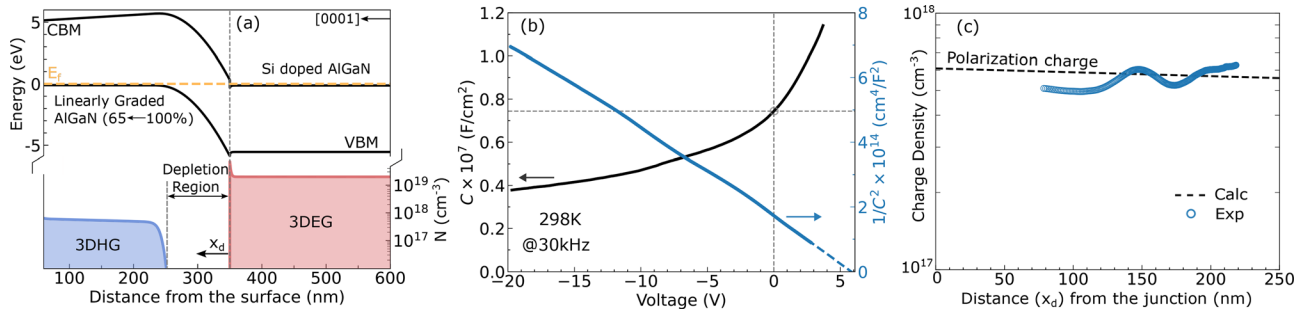

FIG. 3. (a) Energy band diagram and free electron and hole concentration of the p–n diode at zero bias. (b) Room-temperature capacitance–voltage measurements at 30 kHz AC frequency. (c) The extracted charge-density profile in the graded AlGaN layer using Eq. (4), which matches well with the polarization charge calculations done using Eqs. (2) and (3).

doped with donors, the combination gives rise to a two-dimensional electron gas (2DEG) of density $\sim 1.64 \times 10^{13}\,\mathrm{cm}^{-2}$ at the heterojunction. Because of this n-type *accumulation* region, the depletion region falls completely in the p-side. Furthermore, the mobile holes in the linearly graded AlGaN layer are due to distributed polarization doping. Thus, capacitance–voltage (CV) profiling should unambiguously extract the charge-density profile in the DPD layer. Despite the quasi-vertical geometry of the diode, it can be considered a parallel plate capacitor since the layers in contact with the n-electrode are approximately equipotential across the surface under reverse bias. The low reverse bias leakage in this device [Fig. 2(a)] enables reliable CV measurements up to −20 V. The dc bias determines the depletion depth, and a 30 mV AC signal at a frequency of 30 kHz was used for the capacitance measurement in a standard parallel capacitance and conductance $C_p - G_p$ model.[38] Figure 3(b) shows the measured capacitance as a function of the applied DC bias at room temperature. The loss tangent $\tan\delta = 2\pi f(C_p/G_p)$ remains below 0.1 in the entire voltage range, ensuring the validity of the data. The built-in voltage of the junction from the extrapolation of $1/C^2$ vs V in Fig. 3(b) is 5.8 V, close to the expected value of 5.5 V.

The 3D bulk polarization charge density in the DPD layer is the sum of both spontaneous and piezoelectric polarizations $P_{tot} = P_{PZ} + P_{SP}$. The piezoelectric polarization of $Al_xGa_{1-x}N$ coherently strained on AlN is[39]

$$P_{PZ}(x) = 2 \times \left(\frac{a_{Al_xGa_{1-x}N} - a_{AlN}}{a_{AlN}}\right) \times \left(e_{31} - e_{33}\frac{c_{13}}{c_{33}}\right), \quad (2)$$

where c_{13} and c_{33} are elastic coefficients and e_{31} and e_{33} are piezoelectric moduli. The values of spontaneous polarization, elastic coefficients, and piezoelectric moduli for AlN and GaN were taken from Table 1 of Ref. 28. The corresponding values for $Al_xGa_{1-x}N$ were obtained by linear interpolation (Vegard's law). The net carrier-density profile in cm^{-3} along the [0001] direction (z axis) is

$$\rho(z) = \frac{1}{q}\nabla \cdot P_{tot} = \frac{1}{q}\frac{\partial P(x(z))}{\partial z}, \quad (3)$$

where $x(z)$ is the graded Al-content profile along the z axis, a linear function in this case. The charge-density at the edge of the depletion region is extracted from the measured CV data of a one-sided abrupt junction[32] as follows:

$$N = \frac{-2}{q\epsilon_s\epsilon_0} \times \left[\frac{1}{d(1/C^2)/dV}\right], \quad (4)$$

where q is the electron charge, ϵ_s is the relative permittivity of the semiconductor at the edge of the depletion region, and ϵ_0 is the permittivity of the vacuum. A constant value of 9.35 was used for ϵ_s corresponding to an average Al composition of 83% in the DPD layer, interpolated between AlN ($\epsilon_s = 9.21$[40]) and GaN ($\epsilon_s = 10.04$[41]). The depletion width in the DPD layer is $W_D = (\epsilon_0\epsilon_s)/C$.

Figure 3(c) shows the experimentally measured and the calculated charge-density profile (dashed line) along the z direction. The experimental average charge density of $5.7 \times 10^{17}\ \mathrm{cm}^{-3}$ is approximately equal to the calculated density of $5.8 \times 10^{17}\ \mathrm{cm}^{-3}$. Thus, the presence of a high-density polarization-induced 3D hole gas close to the theoretically predicted density is observed. The rather interesting oscillations of the charge density observed in all devices are not captured in the simulation. They could originate either due to periodic fluctuations in Al composition, or Friedel oscillations of the three-dimensional hole gas.[42,43] The root of these oscillations will be investigated in a future work. The destructive breakdown of the devices occurred in the range of −55 to −60 V without any passivation and edge termination structure.

Figure 4(a) shows the measured room temperature electroluminescence (EL) collected from the backside of large 400 μm diameter devices at a forward current density of 110 $\mathrm{A/cm}^2$ at room temperature. A peak at 4.78 eV dominates the emission spectrum. Additionally, a far less intense deep-level luminescence peak of energy ~3.4 eV is also observed. To identify the origins of these peaks, room temperature photoluminescence (PL) experiments were also conducted on an $Al_{0.72}Ga_{0.28}N$/AlN sample with the same Si doping density and without the DPD and p-contact layers using a 193 nm ArF excimer laser excitation. The inset in Fig. 4(a) shows a comparison of the EL and PL spectra. It confirms that the dominant emission peak in EL is from interband radiative recombination in the Si-doped $Al_{0.72}Ga_{0.28}N$ layer.

Figure 4(b) shows the calculated energy band diagram of the diode at a junction bias of 5 V, along with the spatially resolved radiative recombination rate, simulated using STR SiLENSe.[44] The purple arrow on the plot indicates the interband transition responsible for the dominant peak in the EL spectra, where the radiative recombination rate is nearly 10^3 times more intense than in the p-DPD layer. The low to non-observable emission from the DPD layer in the EL spectrum is

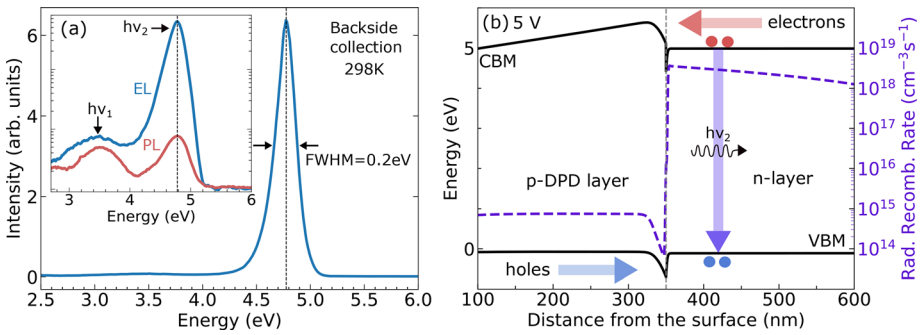

FIG. 4. (a) Room temperature electroluminescence collected from the backside of the device. The inset shows the comparison (in logarithmic scale) between EL from the device and PL from an AlGaN sample with the same composition and doping as the n-layer of the device. (b) Energy band diagram of the diode at 5 V forward bias with the arrow showing the radiative transition corresponding to the main emission peak.

due to two reasons: (1) the product of electron and hole concentrations under forward bias is significantly higher in the n-layer, leading to a higher radiative recombination rate since $R \propto np$, and (2) the luminescence resulting from recombination within the DPD layer has higher energy than the energy bandgap of $Al_{0.72}Ga_{0.28}N$. This means photons emitted in the p-DPD layer moving toward the bulk will be absorbed and re-emitted at a photon energy equal to the n-layer energy bandgap during backside collection.

The weak sub-bandgap peak at approximately 3.4 eV is very close to the energy bandgap of GaN. This peak could be due to optical excitation of the top GaN layer from the emitted 4.8 eV photons, which then make it across the wafer to the backside collector. However, the appearance of a weak 3.4 eV peak in the inset of Fig. 4(a) in the PL spectra of $Al_{0.72}Ga_{0.28}N$ without any GaN layer indicates that the EL peak is also from the n-AlGaN layer. Chichibu *et al.*[45] have proposed the existence of defect complexes consisting of cation vacancies and silicon (V_{III}-nSi_{III}) as an explanation for the deep PL emission bands. These complexes act as self-compensating acceptor-type defects in Si-doped AlN and AlGaN.[46,47] It should be noted that literature reports on luminescence in AlN and AlGaN grown by MBE are scarce,[48–51] and that defect formation may strongly depend on the method of deposition. The presence of these point defects does not affect the calculated polarization charge, since the dispersion in capacitance was less than 10% in the frequency window of ∼1 kHz–1 MHz.

In summary, ultrawide bandgap semiconductor diodes exhibiting low reverse bias leakage and high on/off ratio are realized by MBE, thanks to the low dislocation density of the epilayers grown on bulk AlN substrates. Completely one-sided p–n heterojunction diodes are realized by exploiting polarization-induced doping on the n-side to remove the depletion layer, and distributed polarization doping instead of Mg acceptor doping for the p-type depletion layer. Through capacitance–voltage measurements, the mobile hole concentration and their spatial distribution in the graded AlGaN layers were directly measured and were found to be consistent with what was expected from polarization effects. These polarization-induced ultrawide bandgap semiconductor diodes show stable performance up to 300 °C. The electroluminescence from these diodes is dominated by interband radiative recombination, and deep-level luminescence is greatly suppressed. This suggests the presence of low point defect densities in the MBE grown Si-doped AlGaN layer. Overall, this study demonstrates the flexibility in the design of p–n heterojunction diodes through polarization-induced doping to achieve properties that are not possible in standard diodes. Such heterostructure design that combines bandgap engineering intimately with polarization engineering opens opportunities for more efficient photonic and electronic devices with ultrawide bandgap polar semiconductors than what is possible in nonpolar semiconductors.

The authors thank Takeru Kumabe from the Nagoya University for helpful discussions. This work was supported as part of the Ultra Materials for a Resilient Energy Grid, an Energy Frontier Research Center funded by the U.S. Department of Energy, Office of Science, Basic Energy Sciences under Award No. DE-SC0021230. The authors acknowledge the use of the Cornell NanoScale Facility (CNF), a member of the National Nanotechnology Co-ordinated Infrastructure (NNCI), which was supported by the National Science Foundation (NSF Grant No. NNCI-2025233).

AUTHOR DECLARATIONS

Conflict of Interest

The authors have no conflicts to disclose.

Author Contributions

Shivali Agrawal: Conceptualization (lead); Data curation (lead); Formal analysis (lead); Investigation (lead); Methodology (lead); Writing – original draft (lead); Writing – review & editing (equal). **Len van Deurzen:** Conceptualization (lead); Formal analysis (supporting); Investigation (supporting); Methodology (supporting); Writing – review & editing (equal). **Jimy Encomendero:** Formal analysis (supporting); Investigation (supporting); Methodology (supporting). **Joseph E. Dill:** Investigation (supporting); Methodology (supporting); Writing – review & editing (supporting). **Hsin Wei (Sheena) Huang:** Investigation (supporting); Methodology (supporting). **Vladimir Protasenko:** Investigation (supporting); Methodology (supporting); Writing – review & editing (supporting). **Huili (Grace) Xing:** Conceptualization (equal); Funding acquisition (equal); Project administration (equal); Resources (equal); Supervision (equal); Writing – review & editing (equal). **Debdeep Jena:** Conceptualization (equal); Funding acquisition (equal); Project administration (equal); Resources (equal); Supervision (equal); Writing – review & editing (equal).

DATA AVAILABILITY

The data that support the findings of this study are available from the corresponding author upon reasonable request.

REFERENCES

[1]S. Brochen, J. Brault, S. Chenot, A. Dussaigne, M. Leroux, and B. Damilano, "Dependence of the Mg-related acceptor ionization energy with the acceptor concentration in p-type GaN layers grown by molecular beam epitaxy," Appl. Phys. Lett. **103**, 032102 (2013).

[2]W. Götz, N. M. Johnson, J. Walker, D. P. Bour, and R. A. Street, "Activation of acceptors in Mg-doped GaN grown by metalorganic chemical vapor deposition," Appl. Phys. Lett. **68**, 667–669 (1996).

[3]Y. Taniyasu, M. Kasu, and T. Makimoto, "An aluminium nitride light-emitting diode with a wavelength of 210 nanometres," Nature **441**, 325–328 (2006).

[4]H. Ahmad, J. Lindemuth, Z. Engel, C. M. Matthews, T. M. McCrone, and W. A. Doolittle, "Substantial P-type conductivity of AlN achieved via beryllium doping," Adv. Mater. **33**, 2104497 (2021).

[5]R. Ishii, A. Yoshikawa, M. Funato, and Y. Kawakami, "Revisiting the substitutional Mg acceptor binding energy of AlN," Phys. Rev. B **108**, 035205 (2023).

[6]J. H. Park, D. Y. Kim, E. F. Schubert, J. Cho, and J. K. Kim, "Fundamental limitations of wide-bandgap semiconductors for light-emitting diodes," ACS Energy Lett. **3**, 655–662 (2018).

[7]L. K. Li, M. J. Jurkovic, W. I. Wang, J. M. Van Hove, and P. P. Chow, "Surface polarity dependence of Mg doping in GaN grown by molecular-beam epitaxy," Appl. Phys. Lett. **76**, 1740–1742 (2000).

[8]D. S. Green, E. Haus, F. Wu, L. Chen, U. K. Mishra, and J. S. Speck, "Polarity control during molecular beam epitaxy growth of Mg-doped GaN," J. Vac. Sci. Technol., B **21**, 1804–1811 (2003).

[9]M. Hansen, L. Chen, J. Speck, and S. DenBaars, "Observation of Mg-rich precipitates in the p-type doping of GaN-based laser diodes," Phys. Status Solidi B **228**, 353–356 (2001).

[10]H. Xing, D. S. Green, H. Yu, T. Mates, P. Kozodoy, S. Keller, S. P. DenBaars, and U. K. Mishra, "Memory effect and redistribution of Mg into sequentially regrown GaN layer by metalorganic chemical vapor deposition," Jpn. J. Appl. Phys., Part 1 **42**, 50 (2003).

[11]S. Figge, R. Kröger, T. Böttcher, P. L. Ryder, and D. Hommel, "Magnesium segregation and the formation of pyramidal defects in p-GaN," Appl. Phys. Lett. **81**, 4748–4750 (2002).

[12]Y. Ohba and A. Hatano, "A study on strong memory effects for Mg doping in GaN metalorganic chemical vapor deposition," J. Cryst. Growth **145**, 214–218 (1994).

[13]P. Kozodoy, S. P. DenBaars, and U. K. Mishra, "Depletion region effects in Mg-doped GaN," J. Appl. Phys. **87**, 770–775 (2000).

[14]M. Martens, C. Kuhn, T. Simoneit, S. Hagedorn, A. Knauer, T. Wernicke, M. Weyers, and M. Kneissl, "The effects of magnesium doping on the modal loss in AlGaN-based deep UV lasers," Appl. Phys. Lett. **110**, 081103 (2017).

[15]Z. Zhang, M. Kushimoto, A. Yoshikawa, K. Aoto, C. Sasaoka, L. J. Schowalter, and H. Amano, "Key temperature-dependent characteristics of AlGaN-based UV-C laser diode and demonstration of room-temperature continuous-wave lasing," Appl. Phys. Lett. **121**, 222103 (2022).

[16]Z. Zhang, M. Kushimoto, A. Yoshikawa, K. Aoto, L. J. Schowalter, C. Sasaoka, and H. Amano, "Continuous-wave lasing of AlGaN-based ultraviolet laser diode at 274.8 nm by current injection," Appl. Phys. Express **15**, 041007 (2022).

[17]Z. Zhang, M. Kushimoto, T. Sakai, N. Sugiyama, L. J. Schowalter, C. Sasaoka, and H. Amano, "A 271.8 nm deep-ultraviolet laser diode for room temperature operation," Appl. Phys. Express **12**, 124003 (2019).

[18]S. Tanaka, Y. Ogino, K. Yamada, R. Ogura, S. Teramura, M. Shimokawa, S. Ishizuka, S. Iwayama, K. Sato, H. Miyake, M. Iwaya, T. Takeuchi, and S. Kamiyama, "Low-threshold-current (85 mA) of AlGaN-based UV-B laser diode with refractive-index waveguide structure," Appl. Phys. Express **14**, 094009 (2021).

[19]K. Lee, S. johnsonadwaj, V. Protasenko, H. Xing, and D. Jena, "Efficient InGaN p-contacts for deep-UV light emitting diodes," in *Device Research Conference (DRC)* (IEEE, 2019), pp. 171–172.

[20]T. Kolbe, A. Knauer, J. Rass, H. K. Cho, S. Hagedorn, F. Bilchenko, A. Muhin, J. Ruschel, M. Kneissl, S. Einfeldt, and M. Weyers, "234 nm far-ultraviolet-C light-emitting diodes with polarization-doped hole injection layer," Appl. Phys. Lett. **122**, 191101 (2023).

[21]T. Kumabe, S. Kawasaki, H. Watanabe, S. Nitta, Y. Honda, and H. Amano, "Space–charge profiles and carrier transport properties in dopant-free GaN-based p-n junction formed by distributed polarization doping," Phys. Status Solidi RRL **16**, 2200127 (2022).

[22]K. Nomoto, W. Li, B. Song, Z. Hu, M. Zhu, M. Qi, V. Protasenko, Z. Zhang, M. Pan, X. Gao, H. Marchand, W. Johnson, D. Jena, and H. G. Xing, "Distributed polarization-doped GaN p–n diodes with near-unity ideality factor and avalanche breakdown voltage of 1.25 kV," Appl. Phys. Lett. **120**, 122111 (2022).

[23]Z. Hu, K. Nomoto, B. Song, M. Zhu, M. Qi, M. Pan, X. Gao, V. Protasenko, D. Jena, and H. G. Xing, "Near unity ideality factor and Shockley-Read-Hall lifetime in GaN-on-GaN p-n diodes with avalanche breakdown," Appl. Phys. Lett. **107**, 243501 (2015).

[24]S. Li, M. Ware, J. Wu, P. Minor, Z. Wang, Z. Wu, Y. Jiang, and G. J. Salamo, "Polarization induced pn-junction without dopant in graded AlGaN coherently strained on GaN," Appl. Phys. Lett. **101**, 122103 (2012).

[25]J. Simon, V. Protasenko, C. Lian, H. Xing, and D. Jena, "Polarization-induced hole doping in wide–band-gap uniaxial semiconductor heterostructures," Science **327**, 60–64 (2010).

[26]A. Ahmad, P. Strak, P. Kempisty, K. Sakowski, J. Piechota, Y. Kangawa, I. Grzegory, M. Leszczynski, Z. R. Zytkiewicz, G. Muziol, E. Monroy, A. Kaminska, and S. Krukowski, "Polarization doping—*Ab initio* verification of the concept: Charge conservation and nonlocality," J. Appl. Phys. **132**, 064301 (2022).

[27]R. Chaudhuri, S. J. Bader, Z. Chen, D. A. Muller, H. G. Xing, and D. Jena, "A polarization-induced 2D hole gas in undoped gallium nitride quantum wells," Science **365**, 1454–1457 (2019).

[28]Z. Zhang, M. Kushimoto, M. Horita, N. Sugiyama, L. J. Schowalter, C. Sasaoka, and H. Amano, "Space charge profile study of AlGaN-based p-type distributed polarization doped claddings without impurity doping for UV-C laser diodes," Appl. Phys. Lett. **117**, 152104 (2020).

[29]Z. Zhang, J. Encomendero, R. Chaudhuri, Y. Cho, V. Protasenko, K. Nomoto, K. Lee, M. Toita, H. G. Xing, and D. Jena, "Polarization-induced 2D hole gases in pseudomorphic undoped GaN/AlN heterostructures on single-crystal AlN substrates," Appl. Phys. Lett. **119**, 162104 (2021).

[30]Y. Cho, C. S. Chang, K. Lee, M. Gong, K. Nomoto, M. Toita, L. J. Schowalter, D. A. Muller, D. Jena, and H. G. Xing, "Molecular beam homoepitaxy on bulk AlN enabled by aluminum-assisted surface cleaning," Appl. Phys. Lett. **116**, 172106 (2020).

[31]K. Lee, Y. Cho, L. J. Schowalter, M. Toita, H. G. Xing, and D. Jena, "Surface control and MBE growth diagram for homoepitaxy on single-crystal AlN substrates," Appl. Phys. Lett. **116**, 262102 (2020).

[32]S. M. Sze, Y. Li, and K. K. Ng, *Physics of Semiconductor Devices* (John Wiley & Sons, 2021).

[33]J. M. Shah, Y.-L. Li, T. Gessmann, and E. F. Schubert, "Experimental analysis and theoretical model for anomalously high ideality factors ($n \gg 2.0$) in AlGaN/GaN p-n junction diodes," J. Appl. Phys. **94**, 2627–2630 (2003).

[34]M. S. Ferdous, X. Wang, M. N. Fairchild, and S. D. Hersee, "Effect of threading defects on InGaN/GaN multiple quantum well light emitting diodes," Appl. Phys. Lett. **91**, 231107 (2007).

[35]N. F. Mott, "Conduction in non-crystalline materials," Philos. Mag. A **19**, 835–852 (1969).

[36]C. G. Moe, M. L. Reed, G. A. Garrett, A. V. Sampath, T. Alexander, H. Shen, M. Wraback, Y. Bilenko, M. Shatalov, J. Yang, W. Sun, J. Deng, and R. Gaska, "Current-induced degradation of high performance deep ultraviolet light emitting diodes," Appl. Phys. Lett. **96**, 213512 (2010).

[37]Z. Gong, M. Gaevski, V. Adivarahan, W. Sun, M. Shatalov, and M. Asif Khan, "Optical power degradation mechanisms in AlGaN-based 280 nm deep ultraviolet light-emitting diodes on sapphire," Appl. Phys. Lett. **88**, 121106 (2006).

[38]L. Stauffer, "Fundamentals of semiconductor C-V measurements," Eval. Eng. **47**, 20–24 (2008).

[39]C. Wood and D. Jena, *Polarization Effects in Semiconductors: From Ab Initio Theory to Device Applications* (Springer Science & Business Media, 2007).

[40]M. Feneberg, M. F. Romero, M. Röppischer, C. Cobet, N. Esser, B. Neuschl, K. Thonke, M. Bickermann, and R. Goldhahn, "Anisotropic absorption and emission of bulk $(1\bar{1}00)$ AlN," Phys. Rev. B **87**, 235209 (2013).

[41]M. Feneberg, S. Osterburg, K. Lange, C. Lidig, B. Garke, R. Goldhahn, E. Richter, C. Netzel, M. D. Neumann, N. Esser, S. Fritze, H. Witte, J. Bläsing, A. Dadgar, and A. Krost, "Band gap renormalization and Burstein-Moss effect in silicon- and germanium-doped wurtzite GaN up to 10^{20} cm^{-3}," Phys. Rev. B **90**, 075203 (2014).

[42]K. Kanisawa, M. J. Butcher, H. Yamaguchi, and Y. Hirayama, "Imaging of Friedel oscillation patterns of two-dimensionally accumulated electrons at epitaxially grown InAs(111) *A* surfaces," Phys. Rev. Lett. **86**, 3384–3387 (2001).
[43]M. C. M. M. van der Wielen, A. J. A. van Roij, and H. van Kempen, "Direct observation of Friedel oscillations around incorporated Si_{Ga} dopants in GaAs by low-temperature scanning tunneling microscopy," Phys. Rev. Lett. **76**, 1075–1078 (1996).
[44]See https://www.str-soft.com/devices/silense/ for SiLENSe, STR Group.
[45]S. F. Chichibu, H. Miyake, Y. Ishikawa, M. Tashiro, T. Ohtomo, K. Furusawa, K. Hazu, K. Hiramatsu, and A. Uedono, "Impacts of Si-doping and resultant cation vacancy formation on the luminescence dynamics for the near-band-edge emission of $Al_{0.6}Ga_{0.4}N$ films grown on AlN templates by metalorganic vapor phase epitaxy," J. Appl. Phys. **113**, 213506 (2013).
[46]J. H. Kim, P. Bagheri, R. Kirste, P. Reddy, R. Collazo, and Z. Sitar, "Tracking of point defects in the full compositional range of AlGaN via photoluminescence spectroscopy," Phys. Status Solidi A **220**, 2200390 (2023).
[47]I. Prozheev, F. Mehnke, T. Wernicke, M. Kneissl, and F. Tuomisto, "Electrical compensation and cation vacancies in Al rich Si-doped AlGaN," Appl. Phys. Lett. **117**, 142103 (2020).
[48]L. van Deurzen, J. Singhal, J. Encomendero, N. Pieczulewski, C. S. Chang, Y. Cho, D. A. Muller, H. G. Xing, D. Jena, O. Brandt, and J. Lähnemann, "Excitonic and deep-level emission from N- and Al-polar homoepitaxial AlN grown by molecular beam epitaxy," APL Mater. **11**, 081109 (2023).
[49]M. Kaneko, H. Okumura, R. Ishii, M. Funato, Y. Kawakami, T. Kimoto, and J. Suda, "Optical properties of highly strained AlN coherently grown on 6H-SiC (0001)," Appl. Phys. Express **6**, 062604 (2013).
[50]L. van Deurzen, R. Page, V. Protasenko, K. Nomoto, H. G. Xing, and D. Jena, "Optically pumped deep-UV multimode lasing in AlGaN double heterostructure grown by molecular beam homoepitaxy," AIP Adv. **12**, 035023 (2022).
[51]V. N. Jmerik, E. V. Lutsenko, and S. V. Ivanov, "Plasma-assisted molecular beam epitaxy of AlGaN heterostructures for deep-ultraviolet optically pumped lasers," Phys. Status Solidi A **210**, 439–450 (2013).